34th Annual International Conference of the IEEE EMBS
San Diego, California USA, 28 August - 1 September, 2012

A Framework for Myoarchitecture Analysis of High Resolution Cardiac MRI and Comparison with Diffusion Tensor MRI*

Stephen H. Gilbert, Gregory B. Sands, Ian J. LeGrice, Bruce H. Smaill, Olivier Bernus† and Mark L. Trew†

Abstract— **The ventricular myocardium has a structure of branching laminae through which course regularly orientated myofibers, an architecture important in excitation and contraction. Quantifying this architecture is vital for understanding normal and disease states in the heart and for assessing their impact on electrical function. These data are also highly important in the construction of scientifically and clinically useful computer models of cardiac electrical behavior. Detailed structural information has previously been obtained from serial imaging. In this work we assess the potential for high-resolution (HR) MRI as a means to furnish useful myoarchitecture and compare and contrast this approach with the growing use of DT. Using rat hearts, we conclude that both approaches have strengths and weaknesses, however, HR-MRI may provide a consistently more robust picture of the myoarchitecture in small hearts.**

I. Introduction

The mammalian ventricles have a unique and specialized architecture consisting of a regular helical fiber-orientation which courses through a conserved and complex myolaminar arrangement [1]. Due to the role of these structural features in electrophysiological and biomechanical function in both health and disease, their accurate measurement is important. Changes in fiber orientation and myolaminar sliding are thought to be the principle mechanisms of myocardial thickening in systole [2]. Fiber orientation has long been known to influence the spread of myocardial activation [3], and furthermore, laminar organization has recently been shown to substantially influence activation [4]. Myofiber and myolaminar structure are present throughout the myocardium (except myolaminae are absent in the immediate sub-epicardium [1]) and three principal orthogonal structural directions can be defined: (i) along the fiber axis; (ii) perpendicular to the fiber axis in the laminar plane; and (iii) normal to the laminar plane. This structural arrangement is known as orthotropy [4]. Whole-heart computational modeling requires detailed structural atlases. Ideally these would be from accurate high-throughput 3D imaging but current methods have considerable limitations. Diffusion Tensor - MRI (DT) has been widely used and has been validated for fiber and laminar measurements against 2D methods but it: (i) has limited spatial resolution [5]; (ii) has limited accuracy for laminae [6]; (iii) has not been validated against 3D methods; (iv) is SNR sensitive [5]; (v) the microstructural basis of the DT signal is controversial [7]; and, (vi) the influence of the *b*-value has not been fully explored [7]. HR-MRI has high spatial-resolution, is applicable to the beating heart and it has been validated against 2D-histology [8, 9]. Structure tensor (ST) analysis is an image analysis method which derives a tensor from the distribution of gradient directions within the neighborhood of an image voxel [10, 11]. We hypothesized that ST analysis could be applied to HR-MRI images to quantify fiber and laminar orientation, and that myolaminar orientations from ST would be more accurate and reliable than those from DT, as the largest ST eigenvalue corresponds to the sheet normal direction, whereas in DT it relates to the fiber direction.

Computer models of cardiac arrhythmia are increasingly using high-resolution tissue structure images and experimental recordings from normal and pathological cardiac tissue for validation [12]. These models are used to probe the multi-scale and multi-dimensional structural basis for arrhythmias in a way not possible with experimental recordings alone. Generally electrical activity is simulated using cell membrane models and tissue property parameter sets. Early computational models used histologically determined tissue geometries and fiber orientations or geometries from low resolution MRI [13] and recent models have used geometries and fiber orientations from DT [14], or high-resolution geometries from high-field MRI along fiber and laminar orientations from DT [12]. To the best of our knowledge ventricular fiber and laminar orientations determined directly from HR-MRI have not previously been generated and used for computational electrophysiology simulations. Furthermore, ST and DT determined fiber and laminar orientations have not been compared.

II. Methods

A. Tissue Preparation

Male Wistar rats (N = 5) weighing 200–220 g were euthanized in accordance with the UK Home Office Animals

* This work was supported in part by grants from the Medical Research Council (G0701785, S. H. Gilbert). S.H. Gilbert is the corresponding author
† O. Bernus and M.L. Trew contributed equally to this study.

S.H. Gilbert and O. Bernus are with the Institute of Membrane and Systems Biology, Faculty of Biological Sciences, Multidisciplinary Cardiovascular Research Centre, University of Leeds, Leeds LS2 9JT, United Kingdom phone: +44-113-3431869; fax: +44-113-34342285; e-mail: {s.h.gilbert, o.bernus}@ leeds.ac.uk. S.H. Gilbert and O. Bernus are also with the Inserm U1045 - Centre de Recherche Cardio-Thoracique, L'Institut de rythmologie et modélisation cardiaque, Université Bordeaux Segalen, Centre Hospitalier Universitaire de Bordeaux, PTIB - campus Xavier Arnozan, Avenue du Haut Leveque, 33604 Pessac, France, stephen.gilbert@chu-bordeaux.fr, olivier.bernus@u-bordeaux2.fr.

G.B. Sands, M.L Trew. I.J. LeGrice and B.H.Smaill are with the Auckland Bioengineering Institute, The University of Auckland, UniServices House, Level 6, 70 Symonds Street, City Campus, Auckland 1010, New Zealand, Auckland, New Zealand. B.H. Smaill is also with the Department of Physiology, University of Auckland, Auckland, New Zealand.

(Scientific Procedures) Act 1986 and the hearts were removed and retrograde perfused (as in [9]) with: (i) HEPES-Tyrodes to clear blood; (ii) BDM to prevent contraction; then (iii) MRI contrast agent (0.1% Gd-DTPA) and fixative (4% formaldehyde). Hearts were imaged within 12 hours of fixation.

B. HR-MRI and DT Acquisition and Reconstruction

All hearts were imaged at 20°C using a FLASH (Fast Low Angle SHot) MRI sequence in a Bruker (Ettlingen, Germany) 9.4T spectroscope with echo time (TE) = 7.9 ms, repetition time (TR) = 50 ms, and 20 averages, taking 18h to acquire at a resolution of 50 x 50 x 50 µm. DT imaging was performed using the same spectroscope with a set of 6 optimized directions using a 3D diffusion-weighted spin-echo sequence with TE = 15 ms, TR = 500 ms, taking 2h to acquire at a resolution of 200 x 200 x 200 µm.

C. HR-MRI Preprocessing for Structure Tensor Analysis

A binary mask was created slice-wise from the segmented images by thresholding intensity values and fractional anisotropy and performing a sequence of morphological operations in the following order: clean (removing isolated foreground pixels), bridge (connect pixels separated by one background pixel), fill (fill isolated background pixels), open (binary opening) and a thicken (add pixels around the exterior of an object but do not connect previously unconnected pixels). To avoid undue influence on structural orientation calculations, boundaries at the interface between tissue and non-tissue regions in the MRI images were smoothed as follows. The segmented 3D MR image tissue masks were eroded using a spherical neighborhood of diameter 9 voxels. This ensured that possible non-tissue artifact on the boundaries was removed. A test surface approximately 7 voxels Euclidian distance from the eroded mask was found and the location of the nearest tissue intensity value corresponding to each test voxel was recorded as a comparison voxel value. The tissue intensity values corresponding to the eroded mask were used to provide boundary conditions for a 3D isotropic iterative diffusion filter. The boundary conditions on the image borders were no-flux. Diffusion filtering was not applied to the masked tissue regions – these remained fixed at the tissue intensity values. Diffusion steps were continued until the mean intensity of the test surface voxels corresponded to the mean intensity of the tissue comparison voxels. Typically this required around 150 to 200 iterations (requiring < 5 min on a dual quad-core 2.5 GHz workstation). The resulting images retained the tissue intensity detail in the tissue mask region and had a smooth intensity gradient toward the image background (Fig. 1).

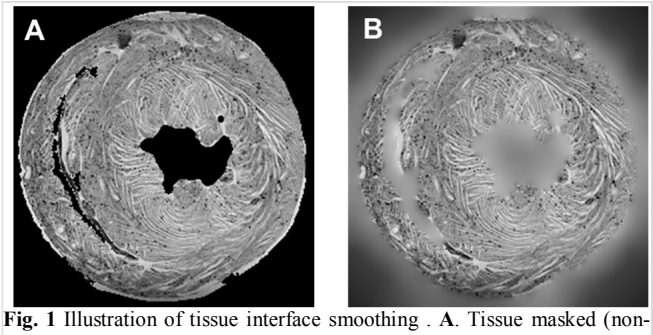

Fig. 1 Illustration of tissue interface smoothing . **A**. Tissue masked (non-eroded) MR image. **B**. Boundary smoothed eroded image, which retains the tissue detail but boundary gradients are de-emphasized

D. Structure Tensor Analysis of High Resolution MR Images

Myostructural orientations were computed from the cleaned images by computing intensity gradients with an optimal 5×5×5 point derivative template [15]. The template was applied to the full 3D image using 1D FFT convolution. The structure tensor (the outer product of the intensity gradient vectors) was computed for each voxel in the 3D image. A sequence of structure tensors at progressive resolution doubling (i.e. 100 µm, 200 µm, 400 µm, etc.) was determined using a level 4 binomial filter. These calculations are completed in around 1 minute. The 200 µm smoothed structure tensor data set (64×64×128 tensors) was used to best match the DT resolution. Eigenanalysis was used to extract the principal directions from the structure tensor at each discrete point (the calculation requires < 10 s) [16]. The eigenvector corresponding to the largest magnitude eigenvalue was taken as the laminae normal direction and the eigenvector corresponding to the smallest magnitude eigenvalue was taken as the fiber direction.

E. Comparison of Structure Tensor and Diffusion Tensor Orientations

A model cardiac geometry, with a manually fitted LV long-axis, was registered to each heart MRI by affine registration (using the Insight Tool Kit, fast affine registration, as implemented in Slicer3) with 20 histogram bins, 40000 spatial samples and 4000 iterations. These steps are shown in Fig. 2. The registered model hence defines: (i) the long-axis (LA) centroid of a cylindrical coordinate system for which the elevation and azimuth angles of the eigenvectors were calculated; and, (ii) selected regions of interest (ROI) for quantification. The orientation angles reported are defined in detail in [17]. Elevation angles are measured from the cardiac short-axis (SA) plane. The fiber helix angle (α_H) is the angle between the transverse plane and the projection of the fiber vector onto the circumferential-longitudinal plane. The fiber transverse angle (α_T) is the angle between the circumferential-longitudinal plane and the projection of the fiber vector onto the transverse plane. The angle between the transverse plane and the projection of the laminar vector

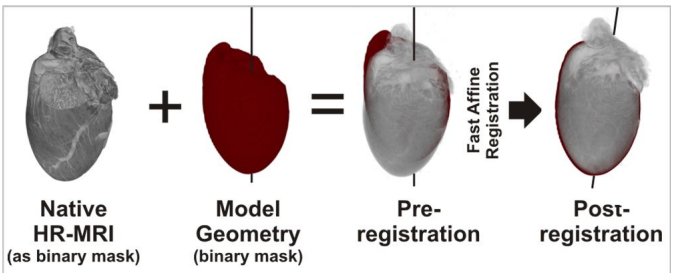

Fig. 2 Fitting a standard model to individual HR-MRI images.

onto the radial-longitudinal plane is B'_S. The angle between the longitudinal—radial plane and the projection of the laminar vector onto the transverse plane B''_S. The angles B'_N and B''_N correspond to B'_S and B''_S but are the orientations of the normal of the laminar plane.

III. Results

The DT data was faster to acquire compared to the HR-MRI data and automated reconstruction of orientation angle maps was faster for the DT than ST data (Table 1).

TABLE I. DT and ST Acquisition and Processing Times

Time (h)[a]	Imaging Approach	
	DT	*HR-MRI/ST*
Aquisistion	2	18
Processing	0.1	0.2

a. on a dual quad-core 2.5 GHz workstation.

Short-axis pseudo-colored angle maps are shown in Fig. 3 alongside the corresponding HR-MRI images for a selected equatorial slice. The selected slice was picked in the model geometry and the corresponding slice was located in each HR-MRI after registration, therefore there was no selection bias which could accompany operator slice selection. The fiber helix angle (α_H) and transverse angle (α_T) have strikingly similar angle distributions across the entire short-axis slice in all hearts, although SNR does vary between the hearts. The relationship between the ST and DT determined laminar normal orientation is more complex: (i) there are regions of strong similarity (e.g. region in the magenta box); and, (ii) regions of markedly different orientation (e.g. the region in the black box). Fig 4 shows transmural angle profiles and pair wise angle difference plots generated from the 5 hearts. These profiles are from the lateral LV (indicated by the orange line on the A2 HR-MRI panel in Fig. 3). The pair wise angle difference plots do not measure the similarity between the structures of the hearts, and instead only compare the orientations measured by ST and DT in individual hearts. The similarity in the DT and ST fiber orientation is striking, both in the transmural profiles and in the angle difference plots. The average difference between the methods is 9±8° for α_H and 12±11° for α_T. Unlike fiber angles, laminar angles can have large changes over small distances [9]. As a consequence transmural profiles are not an ideal approach for comparing laminar orientation between hearts, where small inter-individual differences in laminar architecture are compounded by small registration errors. This consideration accounts for the large differences and s.d. between the laminar normal elevation and azimuth angles for both ST and DT transmural profiles. There are regions of marked difference in mean laminar normal angles, and the pair wise angle difference maps show marked difference between the orientations determined by ST and DT. The average difference between the methods is 34±27° for B'_N and 31±27° for B''_N.

IV. Discussion

The transmural myofiber orientations determined by ST applied to HR-MRI are strikingly similar to DT determined

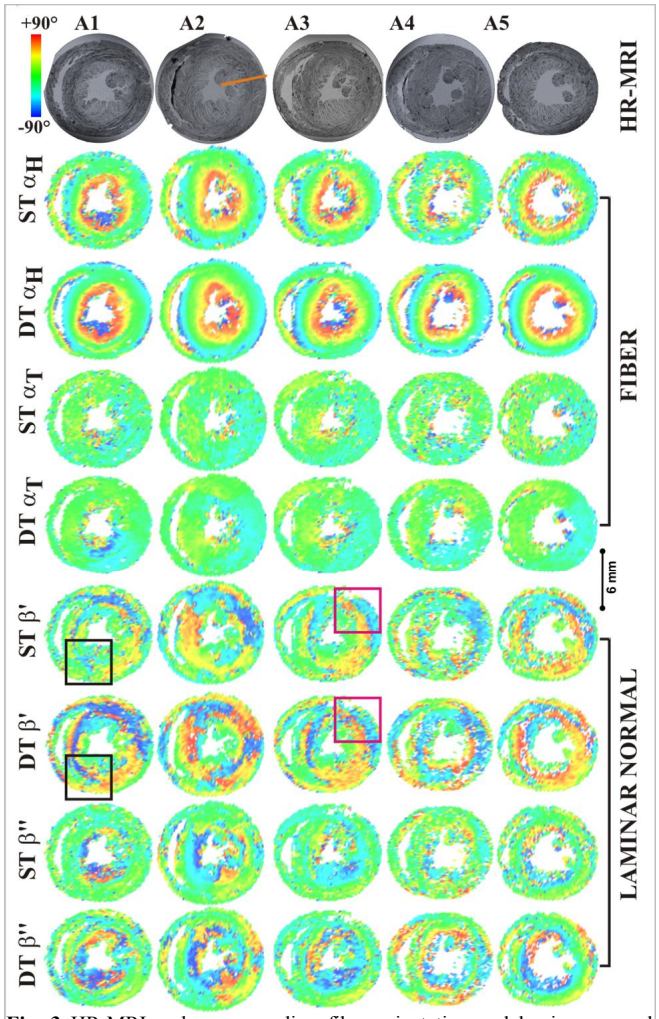

Fig. 3 HR-MRI and corresponding fiber orientation and laminar normal orientation maps for a selected equatorial short-axis slice of five rat hearts. Regions of similar and differing laminar normal orientation are shown in the magenta and black boxes respectively. The orange transmural line on the A2 HR-MRI image indicates the region quantified in Fig. 4.

transmural distributions. Although laminar normal orientations maps show broadly similar angle distributions, close examination reveals regions of differing DT and ST determined orientation, and transmural and angle difference plots show that these differences are substantial. There is not a rigorous theoretical framework and experimental validation of DT measurement of myolaminar orientation. It was proposed [18] that the secondary/tertiary eigenvector correspond to the laminae/laminar normal orientation, but these patterns of diffusion have not been validated on a microstructural scale. The validation of DT laminar measurement has depended on 2D studies with comparison against histology. In a recent study the difference between histologically and DT determined sheet angles was reported as 8° ± 27° [7]. Although the mean difference is relatively small, the standard deviation in the measurements of the sheet angles is quite large, which could be due to inherent limitation of the DT technique, and/or due to the substantial distortion of tissue, which accompanies sectional histological laminar orientation. It is our view that the laminar architecture can be much more reliably assessed using the volumetric HR-MRI

method with no myocardial distortion or damage. We have proposed a framework for myolaminar orientation measurement which: (i) can be used for *in situ* validation of DT; (ii) can directly replace DT. There are some limitations in this preliminary study. It is possible that greater numbers of diffusion directions, greater numbers of repetitions, alternative b-values or alternative voxel sizes may increase the accuracy of DT applied to the myocardium, and a detailed sensitivity analysis has not yet been reported. In this study we assess the performance of 6 directions DT, but recent evidence suggests that this has comparable robustness to 30- or 60-

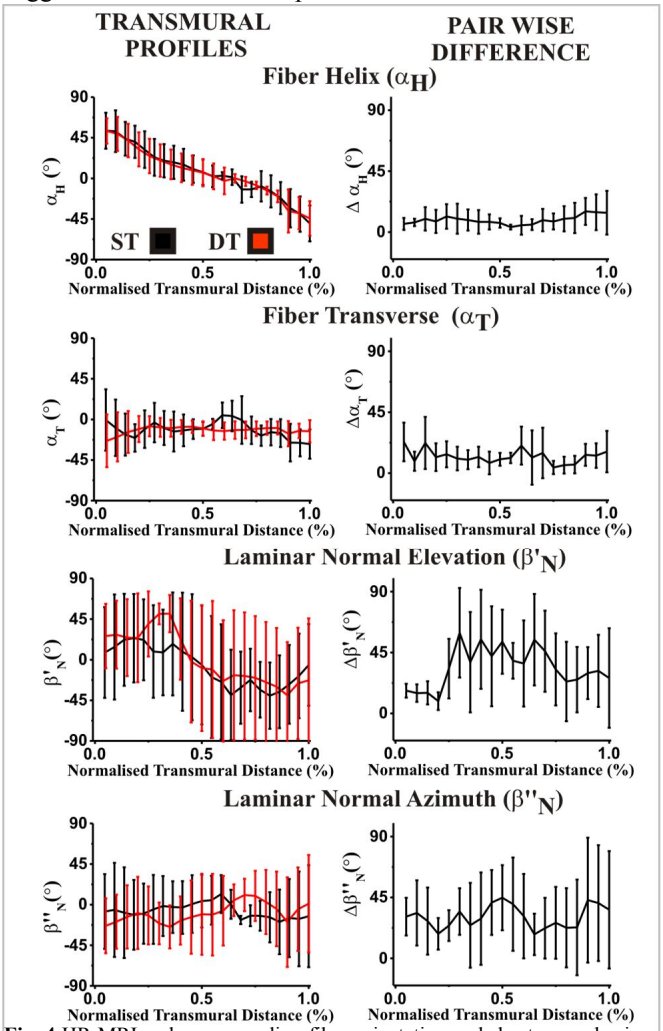

Fig. 4 HR-MRI and corresponding fiber orientation and sheet normal orientation maps for a selected transmural region of an equatorial short-axis slice of five rat hearts. Error bars are mean±s.d.

direction data [18]. Transmural laminar orientation profiles (Fig. 4) do not allow discrimination between a single laminar orientation with high variability and closely located regions of highly different laminar orientation. This will be addressed in future studies through HR-MRI visualization alongside ST and DT measurements. Future studies will also incorporate sensitivity analysis of both ST and DT. Although HR-MRI and ST requires a longer time (~1 day) compared to DT (~1 morning), this time difference is not sufficient to mitigate the benefits of HR-MRI/ST. These are the resolution of actual tissue structures and structural orientations that directly quantify the visible images. Based on our results to date, we conclude that the HR-MRI/ST framework is reliable, robust and the preferred option.

REFERENCES

[1] A. J. Pope, G. B. Sands, B. H. Smaill, I. J. LeGrice, "Three-dimensional transmural organization of perimysial collagen in the heart", *Am J Physiol Heart Circ Physiol.* vol. 295, pp. :H1243-H1252, Jul 2008.

[2] K. D. Costa, Y. Takayama, A. D. McCulloch, J. W. Covell, "Laminar fiber architecture and three-dimensional systolic mechanics in canine ventricular myocardium." *Am. J. Physiol.,* vol. 276, pp. H595-607, Feb 1999.

[3] G. Arisi, E. Macchi, S. Baruffi, S. Spaggiari, B. Taccardi, "Potential fields on the ventricular surface of the exposed dog heart during normal excitation." *Circ. Res.,* vol. 52, pp. 706-715, Jun 1983.

[4] D. A. Hooks, M. L. Trew, B. J. Caldwell, G. B. Sands, I. J. LeGrice, B. H. Smaill, "Laminar arrangement of ventricular myocytes influences electrical behavior of the heart", *Circ Res.*, vol. 101, pp. 103-112, Nov 2007.

[5] Y. Jiang, K. Pandya, O. Smithies, E. W. Hsu, "Three-dimensional diffusion tensor microscopy of fixed mouse hearts", *Magn. Reson. Med.,* vol. 52, pp. 453-460, Sep 2004.

[6] G. L. Kung, T.C. Nguyen, A. Itoh, S. Skare, N. B. Ingels Jr, D. C. Miller et al., "The presence of two local myocardial sheet populations confirmed by diffusion tensor MRI and histological validation", *J. Magn. Reson. Imaging.,* vol. 34, pp. 1080-1091, Nov 2011.

[7] E. W. Hsu, D. L. Buckley, J. D. Bui, S. J. Blackband, J. R. Forder, "Two-component diffusion tensor MRI of isolated perfused hearts", *Magn. Reson. Med.*, vol. 45, pp. 1039-1045, Jun 2001.

[8] S. Köhler, K. H. Hiller, C. Waller,P. M. Jakob, W. R. Bauer, A. Haase, "Visualization of myocardial microstructure using high-resolution T*2 imaging at high magnetic field", *Magn. Reson. Med.*, vol. 49, pp. 371-375, Feb 2003.

[9] S. H. Gilbert, D. Benoist , A. P. Benson, E. White, S. F. Tanner, A. V. Holden, H. Dobrzynski, O. Bernus, A. Radjenovic, "Visualization and quantification of whole rat heart laminar structure using high-spatial resolution contrast-enhanced MRI", *Am. J. Physiol. Heart Circ. Physiol,*. Vol. 302, pp. H287-298, Jan 2012.

[10] Jähne B, *Digital image processing*. 6th ed. Springer-Verlag, The Netherlands, 2005.

[11] J. Zhao, T. D. Butters, H. Zhang, A. Pullan, I. J. LeGrice, G. B. Sands, et al., "An image-based model of atrial muscular architecture: Effects of structural anisotropy on electrical activation" , *Circ. Arrhythm. Electrophysiol.*, to be published.

[12] F. Vadakkumpadan, L. J. Rantner, B. Tice, P. Boyle, A. J. Prassl, E. Vigmond, et al., "Image-based models of cardiac structure with applications in arrhythmia and defibrillation studies", *J. Electrocardiol.*, VOL. 42, PP. 157 e1-10, Mar 2009.

[13] R. H. Clayton, A. V. Panfilov, "A guide to modelling cardiac electrical activity in anatomically detailed ventricles", *Prog. Biophys. Mol. Biol.*, vol. 96, pp. 19-43. Jan 2008.

[14] A. P. Benson, O. V. Aslanidi, H. Zhang, A. V. Holden, "The canine virtual ventricular wall: a platform for dissecting pharmacological effects on propagation and arrhythmogenesis", *Prog. Biophys. Mol. Biol.*, vol. 96, pp. 187-208, Jan 2008.

[15] H. Farid, E. P. Simoncelli, "Differentiation of discrete multidimensional signals", *IEEE Trans. Image. Process*. vol. 13, pp. 496-508, Apr 2004.

[16] Dongarra J, Koev P, Li X. Matrix-vector and matrix-matrix multiplications. In: Bai Z, Demmel J, Dongarra J, Ruhe A, van der Vorst H, eds. Templates for the solution of algebraic eigenvalue problems: A practical guide. Philadelphia: SIAM; 2000:320-326.

[17] A. P. Benson, S. H. Gilbert, P. Li, S. M. Newton, A. V. Holden, "Reconstruction and Quantification of Diffusion Tensor Imaging-Derived Cardiac Fibre and Sheet Structure in Ventricular Regions used in Studies of Excitation Propagation", *Math. Model. Nat. Pheno.*, vol. 3, pp. 101-130, Feb 2008.

[18] Scollan DF, Holmes A, Winslow R, Forder J. Histological validation of myocardial microstructure obtained from diffusion tensor magnetic resonance imaging. Am J Physiol. 1998; 275; H2308-2318.